ELSEVIER

Mathematical modeling of separation characteristics of a coal-washing spiral

S.K. Das [a,*], K.M. Godiwalla [a], Lopamudra Panda [a], K.K. Bhattacharya [b], Ratnakar Singh [b], S.P. Mehrotra [c]

[a] *Mathematical Modeling & Simulation Division, National Metallurgical Laboratory, Council of Scientific & Industrial Research, Jamshedpur 831007, India*
[b] *Mineral Processing Division, National Metallurgical Laboratory, Council of Scientific & Industrial Research, Jamshedpur 831007, India*
[c] *Director, National Metallurgical Laboratory, Council of Scientific & Industrial Research, Jamshedpur 831007, India*

Abstract

An improved mathematical model to simulate the particle and flow behavior in a coal-washing spiral has been developed. The modeling framework addresses three main components of the spiral system: (i) geometry of the spiral and its trough, (ii) fluid motion along the curvilinear path of the spiral and (iii) principal forces acting on a particle incorporating "Bagnold effect". This effect has been addressed for both particle–inertial and macro-viscous regimes. The modeling components have been combined seamlessly by assuming that the particles eventually attain dynamic equilibrium in the forward longitudinal direction and static equilibrium in the transverse direction. The resulting force function provides a spectrum of the particle's radial location on the trough according to their size and relative specific gravity. The model predicts relative specific gravity distribution as a function of equilibrium radial position for different particle sizes. It also computes particle size variation as a function of equilibrium radial position for various values of relative specific gravity. Sensitivities of radial equilibrium distribution of particle size and relative specific gravity with respect to mean flow depth have also been investigated. Simulation results validated with the published data, are found to be reasonably consistent. The model provides an analytical tool for understanding of the separation behavior of particles in a coal-washing spiral.
© 2007 Elsevier B.V. All rights reserved.

Keywords: Spiral separator; Coal washing; Separation characteristics; Equilibrium force balance; Mathematical modeling

1. Introduction

Among the gravity separators, the spiral concentrator is considered to be one of the most efficient and simple unit operations. Because of its relative simplicity and high efficiency, it is widely used under a variety of circuit configurations for processing of minerals and coals. Since, its introduction by Humphreys in the 1940's (Thompson and Welker, 1990), spirals have proved to be a cost effective and an efficient means of concentrating a variety of ores. Their success is attributed to the fact that spirals are environment friendly, rugged, compact, and cost effective (Chedgy et al., 1990; Holland-Batt, 1990, 1992; Kapur and Meloy, 1998). Since the 1980s, there has been an increased interest in recovering coal fines and spirals have become a

* Corresponding author. Tel.: +91 657 2273038; fax: +91 657 2270527.
E-mail address: skd@nmlindia.org (S.K. Das).

common method for the concentration of 0.1 mm to 2 mm coal. Spirals are able to maintain high combustible recoveries while treating material too coarse for flotation and too fine for dense-media separation.

The generic geometry of spiral concentrators consists of an open trough that spirals vertically downwards in helix configuration about a central axis (Wills, 1992). Feed is introduced at the top of the spiral with a range 15–45% of solids (by weight) and is allowed to flow downward. Complex mechanisms, including the combined effects of different forces, differential particle settling rates, interstitial trickling and possibly hindered-settling (Mills, 1978), affect the stratification of particles. Generally, the high-density material reports to the inner edge of the spiral, while the lower density material reports to the high-wall of the spiral. Classification can also occur, predominantly misplacing the fine, high-density particles to the outer edge of the spiral. The center of the spiral trough contains middling material present in the feed. The schematic cross-section shown in Fig. 1 illustrates this separation process.

Studies have also shown that feed rate, especially the total volumetric flow greatly affects its performance and is among one of the critical factors for determining coal spiral capacity. Investigations (Holland-Batt, 1995) show that, for any feed pulp density there exists an optimum feed rate. Studies (MacNamara et al., 1995) indicate that the spiral performance is considerably affected by slurry density and that a more dominant control is observed when combining the slurry density with the solid flow rate. As the volumetric feed rate increases, an increasing amount of entrained material reports to the outer wall, reducing the efficiency.

Until recently, quantitative modeling of spiral performance have met with limited success (Holland-Batt, 1994, 1995, 1998; MacNamara et al., 1995). Since, the conventional empirical approaches for performance analysis based on plant experience have reached almost near saturation, no further significant improvement is expected by exclusive empirical methods.

In this paper, an improved analytical model incorporating Bagnold effect is proposed as a modification to the earlier approach by Kapur and Meloy (1999, 1998). The model equations were reformulated to calculate the mean flow depth, relative specific gravity of the particle and particle size as a function of design and operating parameters of the spiral. Sensitivity studies of the operating parameters on the segregation behavior of particles across the radial width of the trough during their motion along the spiral have been carried out. It is believed that the model reasonably mimics the segregation behavior of a particle during its motion along the spiral with a reasonable degree of realism. The model comprises three important aspects of a spiral separator, namely, (i) modeling of spiral geometry, (ii) fluid flow based on semi-empirical sediment transport correlation and (iii) first principle based equilibrium force balance on a particle moving down the spiral along the helical path. These have been incorporated to formulate a hybrid methodology using first principle based approach coupled with semi-empirical correlations.
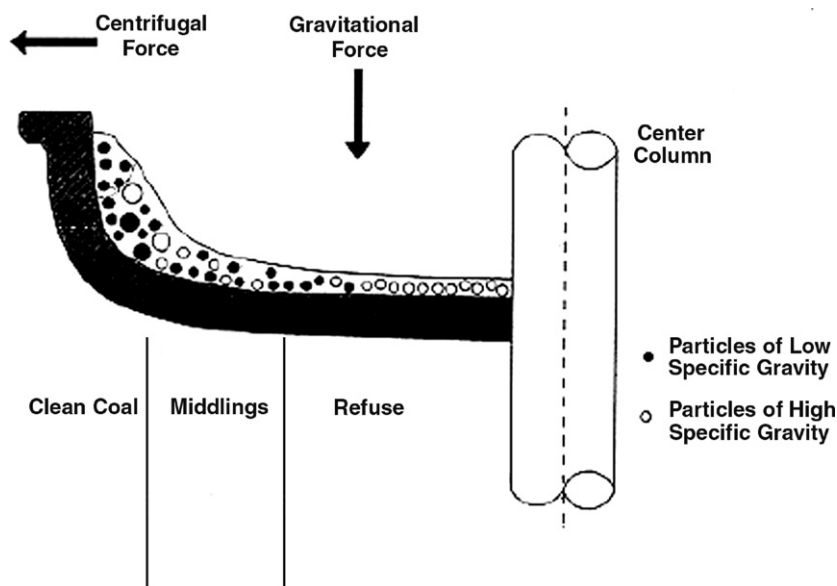

Fig. 1. A sectional view of the a spiral through flow.

2. Process modeling methodology

2.1. Parametric representation of spiral geometry

The performance of the coal-processing spiral is a critical function of its design parameters, which include diameter, height, number of turns, pitch, slope, shape of the trough and its dimension. The model assumes that the deck of the channel comprises an envelope having a large number of axially adjacent helical curves, which are non-intersecting with one another.

The parametric representation of a helix in the Cartesian coordinate system is (Von Seggern, 1990; Krasnov et al., 1990):

$$x = r \sin[\eta] \tag{1}$$

$$y = r \cos[\eta]; \quad 0 \leq \eta \leq N\pi \tag{2}$$

$$z = \frac{U}{2\pi}\eta; \quad 0 \leq z \leq H \tag{3}$$

where, η is a parametric representation of the co-ordinates in Eqs. (1)–(3). Fig. 2 (Kapur and Meloy, 1998) depicts the design parameters of a typical spiral. The longitudinal tangential slope S, at any point on the deck is expressed as

$$S = \tan[\alpha] \tag{4}$$

where, α is the slope angle. The slope, which is also represented as

$$S = \frac{z'(\eta)}{\sqrt{x'(\eta)^2 + y'(\eta)^2}} = \frac{U}{2\pi r} \tag{5}$$

where, x', y' and z' are derivatives of x, y and z with respect to the parameter η. The local slope of the channel deck in the radial or transverse direction is determined by

$$\tan[\theta] = \frac{c_y}{r_o - r_i} \tan \arcsin\left[\frac{r - r_i}{r_o - r_i}\right] \tag{6}$$

where, $r_i \leq r \leq r_o$.

2.2. Treatment of fluid flow on spiral

Spirals exhibit one of the most complex flow regimes among gravity separators. Spiral concentrator flows have a free-surface, shallow depths (<1 cm) and display laminar to increasingly turbulent behaviour. The flow behavior is radially outwards with velocities reaching about 3–4 m/s (Holland-Batt, 1990, 1992, 1994, 1995).

Current understanding of the mechanism of separation on spiral involves primary and secondary flow patterns (Holland-Batt, 1995). These flow patterns allow for dilation of the particle bed and provide an opportunity for separating mechanisms to operate. The primary flow is that of the slurry descending the inclined portion of the trough. Secondary flow occurs radially across the trough. In the upper zone, more fluid layers move away from the center while the lower zone, more concentrated layers (especially where particles are in contact with the solid surface) move towards the center. Density stratification occurs and the secondary flow causes shearing of the strata. This results in bands of higher density particles reporting to the inner region of the trough, whereas lower density particles segregate towards the outer region. A secondary circulation current in a plane perpendicular to the mainstream flow direction, induced by the spiral curvature and the resultant centrifugal force travels outwards near the free-surface. The same resultant force travels towards the central column near the trough base in the inward direction.

In the particulate flow system of a spiral, fluid driven particles move by one or more of the following modes: sliding, rolling and saltation. This process is collectively named as bed-load transport under suspended conditions. The fluid
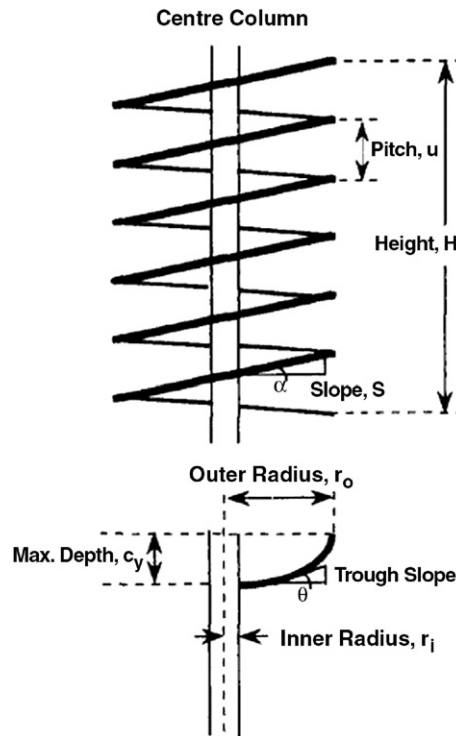
Fig. 2. Geometric/design parameters of a spiral.

dynamics in the spiral can be represented by the Reynolds-averaged turbulent Navier–Stokes equations. In general, when modeling of such type of flows, the fluid phase is considered to be Newtonian and possessing constant physical properties.

The equation of conservation of mass (continuity) is

$$\frac{\partial \rho u_i}{\partial x_i} = 0 \tag{7}$$

The steady-state equations for the conservation of momentum in generalized curvilinear form for a spiral is expressed as

$$\frac{\partial}{\partial x_i}\left(\rho u_i u_j\right) = -\frac{\partial P}{\partial x_i} + \rho g_i + \frac{\partial}{\partial x_i}\left[\mu_{eff}\left(\frac{\partial u_i}{\partial x_j} + \frac{\partial u_j}{\partial x_i}\right)\right] \tag{8}$$

To incorporate the effects of turbulence, an appropriate turbulence models such as, the Renormalization Group (RNG) based (K-ε) model or Large Eddy Simulation (LES) model may be employed in conjunction with the conservation Eqs. (7) and (8).

Computational Fluid Dynamic (CFD) analysis of multi-phase particulate flow and particle dynamics in a spiral is a formidable task. Appropriate equations and turbulence model have not yet been reported for comprehensive two-phase particulate flow analysis for the spiral in the literature. Without multiphase sediment transport simulation (Bagnold, 1966) and non-Newtonian flow considerations, the computational results are unlikely to be commensurate with enormous computational time required for undertaking CFD calculations.

2.2.1. Power law formalism for flow analysis

A more practical approach to flow modeling in a spiral relies on velocity profiles by assuming appropriate flow regimes (Holland-Batt, 1998; MacNamara et al., 1996; Walsh and Kelly, 1992; Weldon and MacHunter, 1997). The action of centrifugal force on water during the flow along the helical path of spiral has two important consequences. The water level at the outer concave wall of the trough exceeds that at the inner convex surface. A transverse secondary

circulation is generated in the form of a helical spiral and its forward movement is analogous to a corkscrew motion. The angles that the inward and the outward-bound flows make with the mean axial flow are functions of depth and radial position. The reported measurements (Holland-Batt, 1990; Holtham, 1990) for these angles have only limited accuracy. The following assumptions are made for the present flow analysis:

- The liquid is considered as an incompressible Newtonian fluid having constant density, viscosity and temperature.
- Surface tension effects are ignored.
- The flow on the spiral is helically symmetrical.

The following expression widely quoted in hydrology literature (Kapur and Meloy, 1998, 1999; Simons and Senturk, 1976; Sivamohan and Forssberg, 1985) for determining the mean deviation angle δ, has been used in this analysis and is given by

$$\tan[\delta] = 11\frac{h}{r} \tag{9}$$

An averaging approach (Holtham, 1990, 1992a,b) was employed in place of classical momentum conservation principle as a matter of practical expediency.

Flow of fluids and sediments in open channels are described by a spectrum of power law relationships whose generalized form is given as (Chen, 1991)

$$V_{\text{mean}} = KR^aS^b \tag{10}$$

The exponents 'a' and 'b' depend on the flow regimes. These flows are categorized as laminar, Maning laminar, Lacey rough channel, Blasius turbulent, Bagnold suspension, transitional or mixed type or a combination thereof (MacNamara et al., 1996). The transitional or mixed flow equation has been employed to describe the flow behavior (Kapur and Meloy, 1998, 1999) of a coal processing spiral. The energy dissipation occurs by the composite interaction of viscosity and turbulence at shallow depths. The mean flow velocities calculated using this equation are in reasonable agreement with those experimentally measured (Chen, 1991). However, the computed flow depths are sometimes overestimated with respect to the reported experimental values. The power law for transitional or mixed flow is expressed as (Holtham, 1990, 1992a,b; Kapur and Meloy, 1998, 1999)

$$V_{\text{mean}} = \frac{26.4}{d_p^{1/6}}R\sqrt{S} \tag{11}$$

where, d_p is a percentile size in the solid feed. Another elementary expression for the mean flow velocity is

$$V_{\text{mean}} = \frac{Q}{A} \tag{12}$$

Measurements on spiral reported in the literature (Holtham, 1990, 1992a,b) demonstrate that the depth of flow increases from about 1 mm at the inner end of the spiral to 8–10 mm or more near the outer end depending upon the feed rate and the spiral design. For ease of calculation of flow parameters, the concept of mean flow depth which is the average depth of the flow across the radial width of the spiral, i.e. $(r_o - r_i)$ was utilized.

The tangential slope, S in Eq. (10) and which is designated as S_m, represents the channel tangential slope at the mid point. This has been substituted in conjunction with appropriate expressions for R and A in terms of the trough geometry and mean flow depth h_m. Finally, V has been eliminated in Eqs. (10) and (11). The flow rate is estimated using the expression

$$Q(x) = K \int_0^{\pi/2} -\frac{\Delta A^2}{\Delta \Omega^2} \frac{1}{\sqrt{C_x^2 - x^2}} S^{1/2} dx \tag{13}$$

where $\quad \Delta\Omega = \left(\left[\frac{dx}{d\eta}\right]^2 + \left[\frac{dy}{d\eta}\right]^2 \right)^{1/2}$ (14)
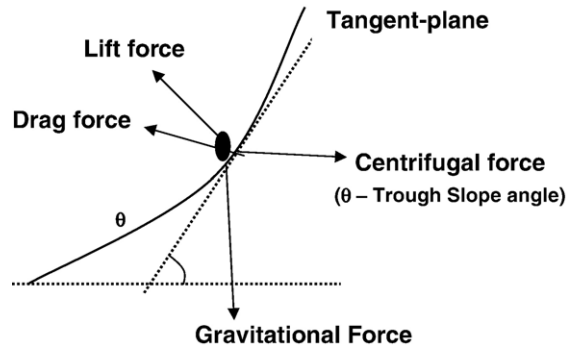
Fig. 3. Principal forces acting on the particle moving on the helical path.

In the above expression, $\triangle\Omega$ is the total wetted perimeter and $\triangle A$ is the differential cross-sectional area (Kapur and Meloy, 1998; Loveday and Cilliers, 1994). Eq. (13) is further modified to arrive at the following governing equation for calculating the total flow rate

$$Q = \frac{3.3\pi^{1.5}}{2d_p^{1/6}} \sqrt{\frac{U}{c_x}} \frac{\left[c_x c_y - (c_x - h_m)(c_y - h_m)\right]^2}{\int_0^{\pi/2} \sqrt{(x'^2 + y'^2)}d\eta + h_m} \tag{15}$$

The integral in Eq. (15) is evaluated as

$$\int_0^{\pi/2} \sqrt{(x'^2 + y'^2)}d\eta = r\pi/2 \tag{16}$$

Substitution of this value in Eq. (15) gives the final expression for the volumetric feed rate (Q) as

$$Q = \frac{3.3\pi^{1.5}}{2d_p^{1/6}} \sqrt{\frac{U}{c_x}} \frac{\left[c_x c_y - (c_x - h_m)(c_y - h_m)\right]^2}{r\pi/2 + h_m} \tag{17}$$

The final governing equation for calculation of mean flow depth h_m, is derived from Eq. (17) as the following polynomial equation given by

$$h_m^4 - 2(c_x + c_y)h_m^3 + (c_x + c_y)^2 h_m^2 - \frac{Q\left(2d_p^{1/6}\right)}{3.3\pi^{1.5}\left(\frac{U}{c_x}\right)^{1/2}} h_m - \frac{Q\left(2d_p^{1/6}\right)}{3.3\pi^{1.5}\left(\frac{U}{c_x}\right)^{1/2}} \pi r_m = 0 \tag{18}$$

where, r_m is mean radial position from the central line. The coefficients of the above equation contain design and operating parameters of the spiral.

2.3. Mechanistic force balance analysis

The forces acting on a particle during its motion in the spiral separator controls the overall dynamics of the particle and its segregation behavior. It is not easy to identify and quantify most of these forces precisely. In general, only rough estimates of the five principal forces, namely, gravity, centrifugal, drag, lift and friction forces can be made (Kapur and Meloy, 1998, 1999; Wills, 1992). In addition, "Bagnold effect" arises at relatively high pulp densities of the feed. Fig. 3

shows a schematic of different principal forces simultaneously acting on a particle during its motion on the spiral trough.

i) Gravity force: Force of gravity (F_g) acting on a particle of diameter (d_p) and density σ which is submerged in a fluid of density ρ, is given as

$$F_g = \frac{\pi}{6}d_p^3(\sigma - \rho)g \tag{19}$$

ii) Centrifugal force: A submerged particle moving with a velocity v_p in a helical path of radius r experiences a centrifugal force (F_c), which is expressed as

$$F_c = \frac{\pi}{6}\frac{d_p^3(\sigma - \rho)v_p^2}{r} \tag{20}$$

However, the velocity of a particle is different from that of the surrounding fluid and varies depending on its size, density, radial location and submergence depth of the flow.

iii) Drag force: The drag force is exerted on the particle in a flow field because of the skin friction and pressure differential between the upstream and the downstream flow conditions. The expression for the drag force is

$$F_d = \frac{\pi \rho g}{4}d_p^2 h \sin[\alpha] \tag{21}$$

The slope angle α, in general, varies over a range of 0.2 to 0.5 rad. The order of magnitude of the drag force is comparable to the gravity force over a broad region of particle size and density.

iv) Lift force: It is observed in river hydraulics and sediment transport studies, that particles traveling slower than the surrounding fluid at a free separation distance of less than its diameter from the bed surface is acted upon by a normal force. This is attributed to the restriction placed on the motion of the fluid on the underside. In spirals, the lift force acts as a particle bed dilator which lifts the particle of different sizes to the same height in to the high velocity upper layers. The lift force is generated as the fluid between the bed and the particle is slowed down and thus the fluid pressure under the particle rises. The generic expression for lift force as

$$F_l = k_1 F_d \tag{22}$$

Even though the lift force can be directly related to the drag force, it is not plausible to assign an accurate value to the proportionality constant k_1. An experimentally determined (empirical) values, ranging from 0.14 to 1, is usually assigned to k_1 (Simons and Senturk, 1976) for theoretical calculations. This approach is quite rudimentary and more empirical.

v) Friction force: As per the theory of friction, the resistance to the motion of a particle is proportional to the normal components of all forces acting on the particle. The constant of proportionality is the coefficient of static friction, which according to Bagnold is virtually same as the coefficient of dynamic friction under water in sediment transport processes.

The frictional force is related to the normal force

$$F_f = F_N \tan[\phi] \tag{23}$$

The value of $\tan[\Phi]$ is reported in the literature(Chang, 1998) and is of the order of 0.5.

vi) Bagnold force: The Bagnold force (Sivamohan and Forssberg, 1985) is attributed to the velocity distribution along the depth of the flowing film, which gives rise to a distribution of shear rates along the depth of flow. As a result, the Bagnold forces, acting on particles located at different depths and having different sizes and densities are diverse in magnitude for each particle in the pulp (Bagnold, 1954). This force acts to disperse particles and its magnitude is directly proportional to the shear rates and the square of the particle diameter. The Bagnold dispersive force preferentially provides a lift to the coarse, light particles into the high velocity

zones of the flowing pulp which, increases from zero at the solid–liquid interface to a maximum value at the free surface.

A high level of turbulence influences the Bagnold force component and distorts the steady-state flow conditions and spatial uniformity of the pulp. Any transients in the flow field affects the Bagnold force experienced by the particle (Atasoy and Spottiswood, 1995). The Bagnold forces, in principle, acting on particles located at different depths, having different sizes and densities will have different in magnitude for each particle in the pulp. Quantitative analysis of the Bagnold force as a function of particle size distribution is difficult. For all practical purposes, the dispersive Bagnold force may be obtained from the dimensionless number expressed as (Holtham, 1992a)

$$N_{Bg} = \frac{\psi^{1/2} \sigma d_p^2}{\mu} \frac{du}{dy} \quad (\text{for } \psi < 14) \tag{24}$$

$$\psi = \frac{1}{\left(\frac{C_{max}}{C}\right)^{1/3} - 1} \tag{25}$$

Depending on the value of N_{Bg}, two limiting flow regimes are defined by (Bagnold, 1954), consisting of "macro-viscous" ($N_{Bg} < 40$) regime and the "particle inertial" regime ($N_{Bg} < 450$), separated by a transition region (Holtham, 1992a). In the "particle inertia" regime the Bagnold dispersive force on a particle is

$$F_{Bg(\text{int})} = 0.04 \sigma (\psi d_p)^2 \left(\frac{du}{dy}\right)^2 \tag{26}$$

Under the macro-viscous condition, the dispersive force on the particle is given as

$$F_{Bg(vis)} = 2.93 \psi^{3/2} \mu \left(\frac{du}{dy}\right) \tag{27}$$

In the "particle inertia" regime, the interstitial fluid plays a minor role and the dominant effects arise from the particle-particle collisions as the particles of one layer overtake those of an adjacent layer moving with lower velocity. In the macro-viscous regime, the forces are transmitted by interstitial fluid friction and are therefore dependent on fluid viscosity but are independent of particle density and size. The mathematical relationships to describe the flows involved in the separation of particles and to obtain an approximate estimation of the secondary circulation of the pulp that flows down along the spiral separator is reported in the literature (Sivamohan and Forssberg, 1985):

The expression for radial inward velocity u at a fractional flow depth, y_h is

$$u = \frac{v^2 h^2 y_h \left(7 y_h^5 - 42 y_h^4 + 70 y_h^3 - 72 y_h + 32\right)}{210 r \, v \cos\theta} \tag{28}$$

The primary velocity v at fractional depth y_h is

$$v = \frac{y_h (2 - y_h) h^2 U g}{4 \pi r v} \tag{29}$$

The inward flow of the bottom layers and the outward flow of upper layers are connected by rising currents on the inner radius and falling currents on the outer radius. The resulting helical boundary between the upward and downward moving layers is determined by the design of the spiral. The rising currents are significant such that they provide a unique phenomenon by lifting the small particles upwards. This signifies that, if the phenomenon proportionated with Bagnold's effect, the particles of different sizes will be lifted approximately to similar extent (same height), which would alleviate any undesirable separation.

2.4. Force balance with Bagnold effect

The static equilibrium analysis provides an understanding of segregation of particles according to their density and size during their descent along the helical path of the spiral. The longitudinal component of all principal forces F_L, acting on a particle in steady motion is given as (Kapur and Meloy,1998)

$$F_L = F_g \sin[\theta]\sin[\alpha] - F_c \cos[\theta]\sin[\alpha] + F_d \cos[\delta] - F_N \tan[\phi] = 0 \tag{30}$$

The normal component of the force is given as

$$F_N = F_g \cos[\theta] + F_c \sin[\theta] - F_1 \tag{31}$$

The transverse component of forces acting on an immobile particle is

$$F_T = F_c \cos[\theta]\cos[\alpha] + F_d \sin[\delta] - F_g \sin[\theta]\cos[\alpha] = 0 \tag{32}$$

In the earlier model (Kapur and Meloy, 1998), lift force is considered only as a fixed proportion of the drag force under various flow conditions. In the present model, Bagnold effect is incorporated in the equilibrium force balance analysis and modified force balance equations have been derived for both "particle–inertial" and "macro-viscous" regimes.

(i) The force balance for the "particle–inertial" regime ($N_{Bg} > 450$) is

$$\frac{\rho h S}{4\sqrt{1+S^2}} \left[\frac{\cos[\delta] + \sin[\delta]\tan[\alpha] + \tan[\phi]\sec[\alpha]\sin[\delta]\tan[\theta]}{\cos[\theta]\sin[\alpha] + \tan[\phi]\sin[\theta]} \right] = \frac{d_p g \tan[\phi](\sigma - \rho)}{6} \left[\frac{\cos[\theta] + \sin[\theta] + \tan[\theta]}{\cos[\theta]\sin[\alpha] + \tan[\phi]\sin[\theta]} \right]$$
$$- \frac{0.04\sigma(\psi d_p)^2 \frac{du}{dy}}{\cos[\theta]\sin[\alpha] + \tan[\phi]\sin[\theta]}\tan[\theta] \tag{33}$$

(ii) The force balance for the "macro-viscous" regime ($N_{Bg} < 40$) is

$$\frac{\rho h S}{4\sqrt{1+S}} \left[\frac{\cos[\delta] + \sin[\delta]\tan[\alpha] + \tan[\phi]\sec[\alpha]\sin[\delta]\tan[\theta]}{\cos[\delta]\sin[\delta] + \tan[\phi]\sin[\theta]} \right] = \frac{d_p g \tan[\phi](\sigma - \rho)}{6} \left[\frac{\cos[\theta] + \sin[\theta]\tan[\theta]}{\cos[\theta]\sin[\alpha] + \tan[\phi]\sin[\theta]} \right]$$
$$- \frac{2.93\psi^{2/3}\mu\left(\frac{du}{dy}\right)}{\cos[\theta]\sin[\alpha] + \tan[\phi]\sin[\theta]}\tan[\phi] \tag{34}$$

The corresponding expressions for S, angles α, θ and δ, h_m, ψ, du/dy, $F_{Bg(int)}$ and $F_{Bg(vis)}$ may be substituted from Eqs. (4), (6), (18), (25), (26) and (28) to generate further expressions to calculate the relative specific gravity and particle diameter as a function of equilibrium radial position.

For "particle–inertial" regime ($N_{Bg} \geq 450$),

(i) Equilibrium distribution of relative specific gravity

$$\frac{(\sigma - \rho)d_p g}{6\rho} 0.04 \frac{\sigma}{\rho}(\psi d_p)^2 \frac{du}{dy} = \frac{6U h_m \cos\left(\tan^{-1}\left(\frac{C_y}{r_0 - r_i}\tan\arcsin\left[\frac{r-r_i}{r_0-r_i}\right]\right)\right)}{4 d_p g \tan\phi\sqrt{(U)^2 + (2\pi r)^2}} \left[k_1\tan\phi + \cos\left(\tan^{-1}\left(11\frac{h_m}{r}\right)\right) \right.$$
$$+ \left(\sin\left(\tan^{-1}\left(\left(11\frac{h_m}{r}\right)\right)\right)\right)\left(\frac{U}{2\pi r}\right) + \tan\phi\sec\left(\tan^{-1}\left(\frac{U}{2\pi r}\right)\right)$$
$$\times \sin\left(\tan^{-1}\left(11\frac{h_m}{r}\right)\right)\left(\frac{C_y}{r_0 - r_i}\tan\arcsin\left[\frac{r-r_i}{r_0-r_i}\right]\right] \tag{35}$$

(ii) Equilibrium distribution of particle size

$$d_p^2 + \frac{(\sigma - \rho)g d_p}{6\rho A} = \frac{1}{A}\left[\frac{6Uh_m\cos\left(\tan^{-1}\left(\frac{C_y}{r_0-r_i}\right)\tan\arcsin\left[\frac{r-r_i}{r_0-r_i}\right]\right)}{4d_p g\tan\phi\sqrt{(U)^2+(2\pi r)^2}}\left[k_1\tan\phi + \cos\left(\tan^{-1}\left(11\frac{h_m}{r}\right)\right)\right.\right.$$
$$+ \left(\sin\left(\tan^{-1}\left(\left(11\frac{h_m}{r}\right)\right)\right)\left(\frac{U}{2\pi r}\right) + \tan\phi\sec\left(\tan^{-1}\left(\frac{U}{2\pi r}\right)\right)\right)$$
$$\left.\left.\times \sin\left(\tan^{-1}\left(11\frac{h_m}{r}\right)\right)\left(\frac{C_y}{r_0-r_i}\right)\tan\arcsin\left[\frac{r-r_i}{r_0-r_i}\right]\right]\right] \tag{36}$$

where, $A = -\left(0.04\frac{\sigma}{\rho}\psi^2\frac{du}{dy}\right)$
For, "macro-viscous" regime ($N_{\text{Bg}} \le 40$),

(i) Equilibrium distribution of relative specific gravity

$$\frac{(\sigma-\rho)d_p g}{6\rho} - 2.93\psi^{2/3}\mu\left(\frac{du}{dy}\right) = \frac{6Uh_m\cos\left(\tan^{-1}\left(\frac{C_y}{r_0-r_i}\right)\tan\arcsin\left[\frac{r-r_i}{r_0-r_i}\right]\right)}{4d_p g\tan\phi\sqrt{(U)^2+(2\pi r)^2}}\left[k_1\tan\phi + \cos\left(\tan^{-1}\left(11\frac{h_m}{r}\right)\right)\right.$$
$$+ \left(\sin\left(\tan^{-1}\left(\left(11\frac{h_m}{r}\right)\right)\right)\left(\frac{U}{2\pi r}\right) + \tan\phi\sec\left(\tan^{-1}\left(\frac{U}{2\pi r}\right)\right)\right)$$
$$\left.\times \sin\left(\tan^{-1}\left(11\frac{h_m}{r}\right)\right)\left(\frac{C_y}{r_0-r_i}\right)\tan\arcsin\left[\frac{r-r_i}{r_0-r_i}\right]\right] \tag{37}$$

(ii) Equilibrium distribution of particle size

$$d_p = \frac{6\rho}{(\sigma-\rho)}\left[\frac{6Uh_m\cos\left(\tan^{-1}\left(\frac{C_y}{r_0-r_i}\right)\tan\arcsin\left[\frac{r-r_i}{r_0-r_i}\right]\right)}{4d_p g\tan\phi\sqrt{(U)^2+(2\pi r)^2}}\left[k_1\tan\phi + \cos\left(\tan^{-1}\left(11\frac{h_m}{r}\right)\right)\right.\right.$$
$$+ \left(\sin\left(\tan^{-1}\left(\left(11\frac{h_m}{r}\right)\right)\right)\left(\frac{U}{2\pi r}\right) + \tan\phi\sec\left(\tan^{-1}\left(\frac{U}{2\pi r}\right)\right)\right)$$
$$\left.\left.\times \sin\left(\tan^{-1}\left(11\frac{h_m}{r}\right)\right)\left(\frac{C_y}{r_0-r_i}\right)\tan\arcsin\left[\frac{r-r_i}{r_0-r_i}\right]\right]\right] + 2.93\psi^{3/2}\mu\left(\frac{du}{dy}\right) \tag{38}$$

The relative specific gravity is defined as the ratio of difference between particle and water densities and density of water, i.e, $(\sigma-\rho)/\rho$. The relative specific gravity provides a better theoretical understanding of separation behaviour of various particle sizes and their distribution as a function of equilibrium radial position. This parameter is indicative of the relative specific gravity variation during particle segregation across the radial width of the spiral. Since, N_{Bg} belongs to "the particle–inertial" regime (i.e $N_{\text{Bg}} > 450$), Eq. (35) is employed to compute the relative specific gravity as a function of equilibrium position for various particle sizes. Similarly Eq. (36) is employed to compute the particle size as a function of equilibrium position for different relative specific gravities. The estimates of ϕ available in the literature (Chang, 1998; Simons and Senturk, 1976) is incorporated in this model.

3. Numerical implementation

The polynomial Eq. (18) was solved using a modified Newton–Rapson technique and Eqs. (35) and (36) were solved in an iterative manner. The model was implemented in a **C++** code to compute geometric parameters, mean flow depth**,** distribution of relative specific gravity and particle size as a function of radial

Table 1
Design data of the coal-washing spiral

(i) Height (H) = 2.5 m	(ii) Pitch (U) = 0.425 m
(iii) Slope (S) = (tan α) = 0.17	(iv) Outer radius (r_o) = 0.48 m
(v) Inner radius (r_i) = 0.08 m	(vi) Trough slope(tan θ) = 0.2
(vii) Max. depth(c_y) = 0.15 m	(vii) Radial width(c_x) = 0.4 m

equilibrium position. The design data of a typical coal-washing spiral was used in this analysis. The data is given in Table 1. The volumetric feed rate (Q) was taken in the range of 0.3 to 0.6 m³/h for Patherdih (Jharkhand, India) coal fines used in this simulation studies.

4. Results and discussion

Because of the paucity of force equilibrium data in the literature for washing of coal using a spiral separator, the validation of the model was attempted with the published data for a spiral used for processing of heavy mineral. The first principle based force balance philosophy including Bagnold effect and concept of relative specific gravity are equally applicable to any particle irrespective of chemical compositions as the force balance methodology is developed embodying the physics of the problem. Fig. 4 shows the distribution of relative specific gravity as a function of equilibrium radial position, for particle sizes of 1 mm and 1.5 mm. Model predictions are depicted by continuous line and literature values are shown as dashed lines. The model predictions are compared and validated with the published data (Kapur and Meloy, 1998) for identical design and processing conditions and the trends are found to be in reasonable agreement. Though the present model seems to predict a somewhat higher value of relative specific gravity distribution, the model predictions with inclusion of the Bagnold effect in the force balance analysis depicts relatively higher separation behaviour of particles with respect to earlier studies (Kapur and Meloy, 1998).

Figs. 5–7 show the distribution of relative specific gravity as a function of equilibrium radial position for different particle sizes, namely, 1, 1.25, 1.5, 1.75 and 2 mm for mean flow depths of 5, 4 and 3 mm respectively. In each of these figures, distribution of relative specific gravity as a function of equilibrium position monotonically decreases with increase in particle size. The negative slope of these curves, i.e, the gradient of relative specific gravity per unit radial distance $\frac{d}{dr}\left(\frac{\sigma-\rho}{\rho}\right)$, is a measure of the separation efficiency. This means, lower the slope, the greater is the efficiency. It is further depicted that the quantity $\frac{d}{dr}\left(\frac{\sigma-\rho}{\rho}\right)$ is a slow varying function of radial width. This indicates that larger particle size in the range of 1 to 2 mm and higher has better separation characteristics. Fig. 8 shows the distribution of relative specific gravity as a
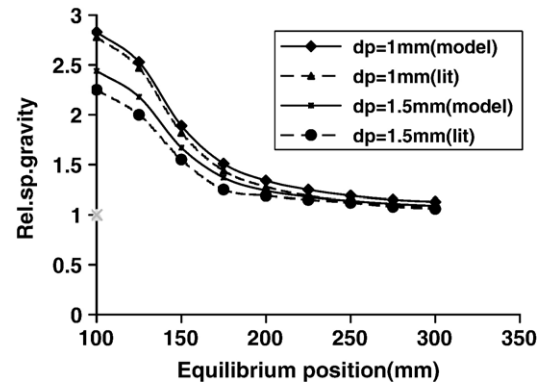

Fig. 4. Predicted radial distribution of relative specific gravity and verification with published literature (Kapur et al., 1998).
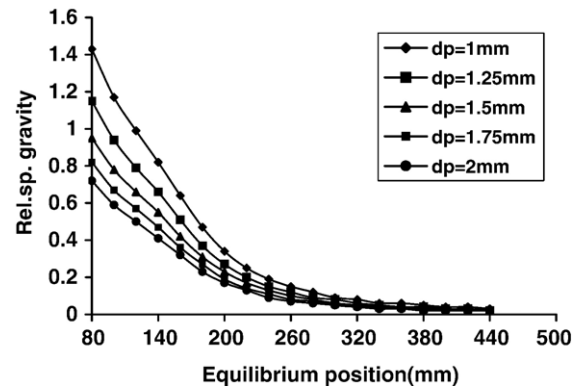

Fig. 5. Effect of particle size variation on the radial distribution of relative specific gravity (feed mean flow depth = 5 mm).
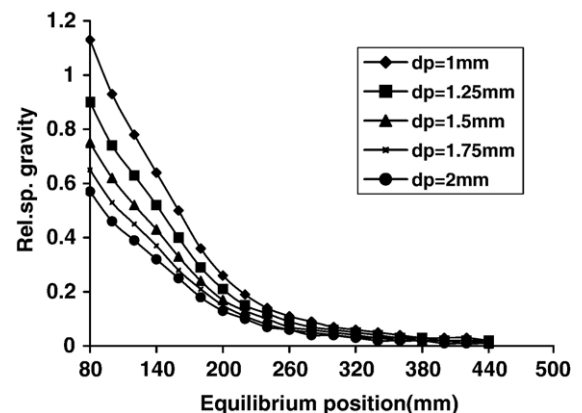

Fig. 6. Effect of particle size variation on the radial distribution of relative specific gravity (feed mean flow depth = 4 mm).
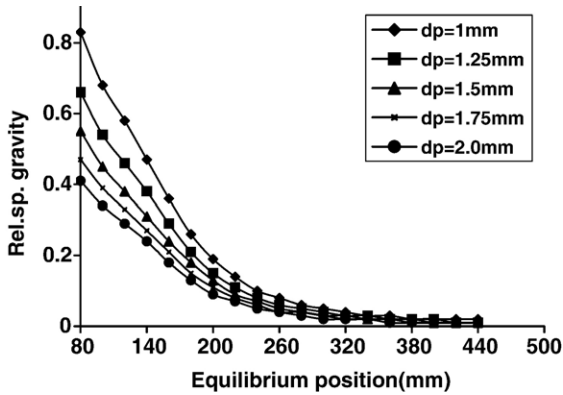
Fig. 7. Effect of particle size variation on the radial distribution of relative specific gravity (feed mean flow depth=3 mm).
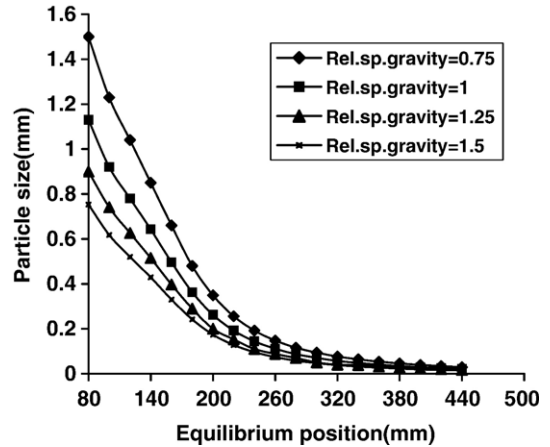

Fig. 10. Effect of relative specific gravity on the radial distribution of particle size (feed mean flow depth=4 mm).
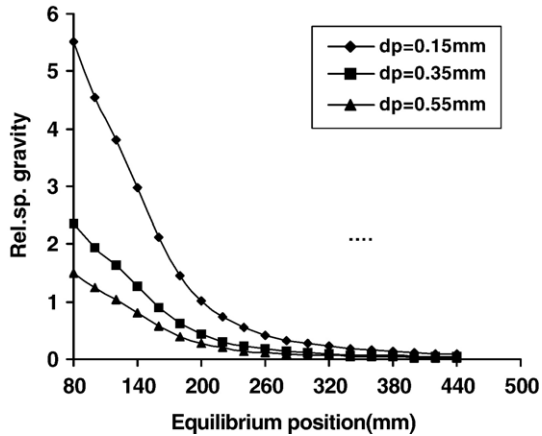

Fig. 8. Effect of small particle size variation on the radial distribution of relative specific gravity (feed mean flow depth=3 mm).

function of equilibrium radial position for different particle sizes, namely, 0.15 mm, 0.35 mm and 0.55 mm for mean flow depth of 3 mm. This figure also depicts distribution of relative specific gravity as a function of equilibrium position, which monotonically decreases with increase in particle size. The model, which is generic in its formulation and is equally applicable for both fine and coarse particle sizes within the specified range (0.1–2 mm). Figs. 9–11 show the distribution of particle sizes as a function of equilibrium radial position for different relative specific gravity, namely, 0.75, 1, 1.25 and 1.5, respectively at various mean flow depths. It is evident that for lower relative specific gravity values, the gradient of particle size distribution along the equilibrium radial distance is higher.

As observed in actual spiral operation and substantiated in these simulation results, that lighter particles (lower ash content) are segregated in the outer region while the heavier particles (higher ash content)
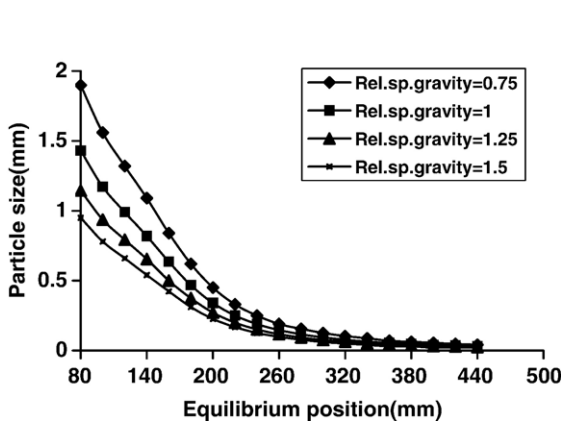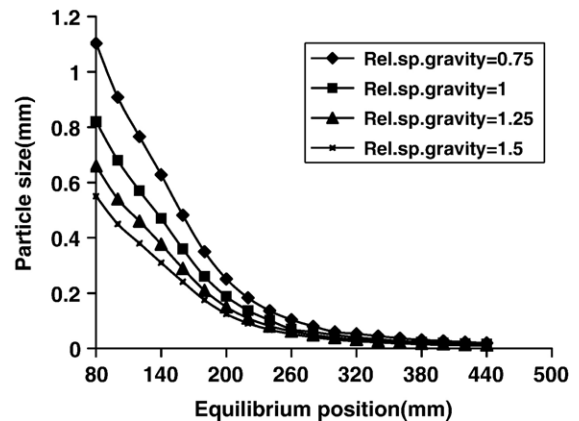

Fig. 9. Effect of relative specific gravity on the radial distribution of particle size (feed mean flow depth=5 mm).

Fig. 11. Effect of relative specific gravity on the radial distribution of particle size (feed mean flow depth=3 mm).
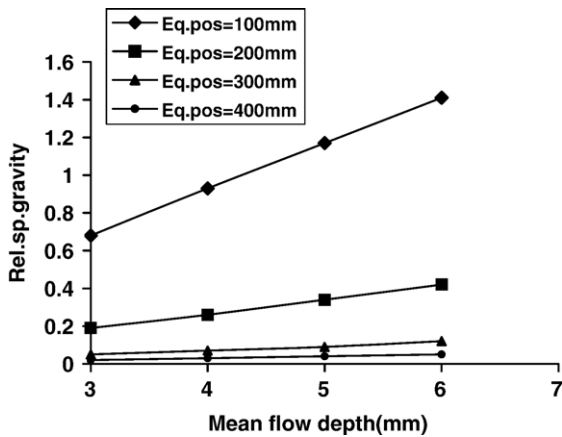
Fig. 12. Sensitivity of relative specific gravity with mean flow depth at various equilibrium positions (particle size=1 mm).

concentrated in the inner region of the trough for all considered values of particle relative specific gravity. The present force equilibrium spiral model, even without tuning the adjustable parameters, yields reasonably realistic values for both particle–fluid relative specific gravities and particle sizes.

Figs. 12–14 show the particle relative specific gravity variation as a function of mean flow depth at various equilibrium positions (100, 200, 300 and 400 mm) for different particle sizes, namely, 1,1.5 and 2 mm, respectively. It is observed that for all radial equilibrium positions, the relative specific gravity decreases with an increase in particle size as a function of mean flow depth. However, the relative specific gravity increases almost linearly with mean flow depth for any given particle size. All the simulation runs have been carried out for "particle–inertial" regime for $N_{Bg} > 450$.
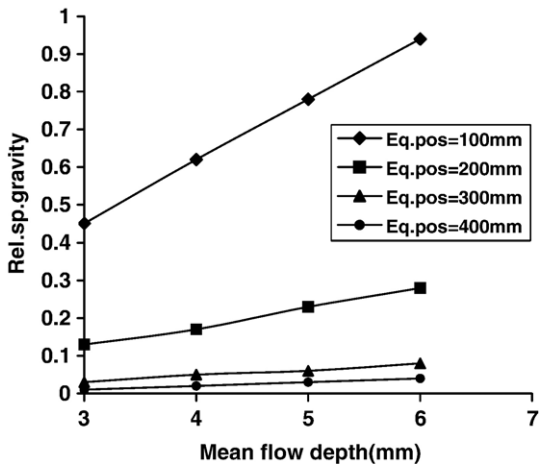

Fig. 13. Sensitivity of relative specific gravity with mean flow depth at various equilibrium position (particle size=1.5 mm).
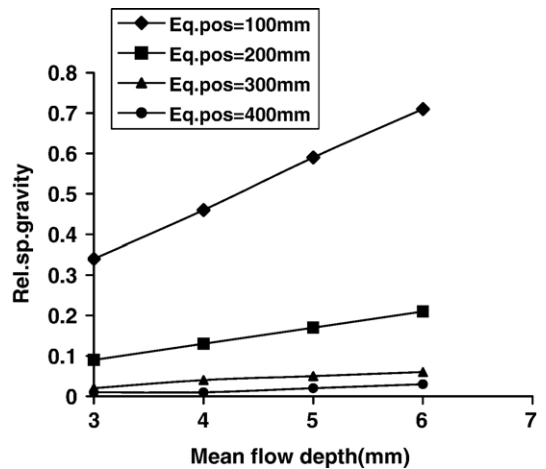

Fig. 14. Sensitivity of relative specific gravity with mean flow depth at various equilibrium position (particle size=2 mm).

The simulation results reported earlier, signify that the conditions under which the "Bagnold force" occurs are very likely to exist in the spiral under normal operating conditions. At low feed pulp density, solid concentrations at some points on the trough of each spiral are sufficient to take the flow into the "particle–inertial" regime. The predictions based on the present model for equilibrium radial distribution of relative specific gravity and its comparison with an earlier model (Kapur and Meloy, 1998) suggest that explicit treatment of Bagnold forces is imperative in the force balance analysis to obtain an improved predictive framework.

5. Conclusion

A spiral model for processing coal is presented. The model incorporates three principal components of equilibrium force balance formulation with Bagnold effect. This is a modification on the earlier model. The components are spiral geometry, flow analysis and a modified force balance approach. This investigation has also shown that it is possible to characterize the separation behavior of an industrial spiral (involving calculation of mean flow depth) using power law formalism of hydrology and approximate flow profile of the trough to account for the Bagnold effect in the force balance formulation. Therefore, rigorous and computation intensive numerical solution of the Navier–Stokes equations for the complex spiral geometry may be avoided as a first approximation. The present model provides an exploratory foray for analysis of spiral separation characteristics and has scope for improvement and refinement. Although, the steady-state attainment of the flow field is a debatable issue, nevertheless, the simulation results suggest that the force

equilibrium methodology including the Bagnold effect could provide a useful simulation framework. This would facilitate better understanding of the separation characteristics in an operating spiral. The semi-empirical approach for fluid dynamic analysis is justified by the need for developing an appropriate force equilibrium model for an operating spiral with a complex spectrum of flow regimes. Further refinement of the quantitative multiphase hydrodynamical description of the spiral without intensive and time consuming computations still remains a challenging task. The results are encouraging to infer that the model presented here is able to reasonably predict separation characteristics of coal-washing spiral in terms of radial equilibrium distribution of relative specific gravity and particle size.

Nomenclature

A	Cross-sectional area of flow
a	Exponents in Eq. (10)
b	Exponents in Eq. (10)
C	Volume concentration of solids
C_{max}	maximum concentration
c_x	$(r_o - r_i)$ radial width of the trough
c_y	Maximum depth of the trough
d_p	Percentile size in the solid feed/particle size
F_g	Force of gravity
F_c	Centrifugal force
F_d	Drag force
F_l	Lift force
F_f	friction force
F_N	normal component of all forces
F_T	Transverse component of forces
F_{Bg}	Bagnold dispersive force
$F_{Bg(int)}$	Bagnold force (particle inertia)
$F_{Bg(vis)}$	Bagnold force (macro viscous)
g_i	Gravitational acceleration
H	Spiral height
h	Depth of the flow
h_m	Mean flow depth
K	Composite resistance coefficient
$k1$	Proportionality constant(Eq. (22))
N	Twice number of turns
N_{Bg}	Bagnolds number
P	Static pressure
Q	Volumetric feed rate
R	Hydraulic radius of the channel
r	Radial distance/equilibrium position
r_i	Inner radii
r_o	Outer radii
r_m	Mean radial position from the central line
S	Longitudinal tangential slope
U	Pitch
u_i, u_j	Cartesian components of the velocity
u	Radial inward velocity at fractional depth
v	Primary velocity at fractional depth
V_{mean}	Mean flow velocity
V_p	Velocity of the particle
x,y,z	Cartesian co-ordinates
x_j	Co-ordinates in Cartesian tensor notations.
y_h	Fractional depth

Greek symbols

η	Geometric parameter representing co-ordinates
θ	Local slope angle
ρ	Fluid density
μ	Dynamic viscosity of the liquid
ψ	Linear concentration
μ_{eff}	Effective viscosity
δ	Mean deviation angle
α	Slope angle
Φ	Constant of proportionality (Eq. (23))
σ	Density of solid particle

Acknowledgement

References

Atasoy, Y., Spottiswood, D.J., 1995. A study of particle separation in a spiral concentrator. Minerals Engineering 8, 1197–1208.

Bagnold, R.A., 1954. Experiments on a gravity free dispersion of large solid spheres in a Newtonian fluid under shear. Proceedings of the Royal Society of London, Set A 225, 49–63.

Bagnold, R.A., 1966. An approach to sediment transport problem from general physics. U.S. Geol. Surv. Prof. Pap. 422–1.

Chang, H.H., 1998. Fluvial Process in River Engineering. John Wiley, New York. (Chapter, 8).

Chedgy, D.G., Placha, D.S., Watters, L.A., 1990. Spiral Concentrators for Fine Coal Processing. PCMIA/SME Joint Meeting, Washington, PA, November 1–2.

Chen, C.L., 1991. Power law of flow Resistance in open channels: Manning's formula revisited. In: Yen, B.C. (Ed.), Channel Flow Resistance: Centennial of Manning's formula. Water Resources Publications, Littleton, pp. 206–240.

Holland-Batt, A.B., 1990. Interpretation of Spiral and Sluice Tests," Trans. Instn. Mining and Metallurgy 99, C1–C20.

Holland-Batt, A.B., 1992. A Study of the Potential for Improved Separation of Fine Particles by Use of Rotating Spirals. Minerals Engineering 5 (10–12), 1099–1112.

Holland-Batt, A.B., 1994. The Effect of Feed Rate on the Performance of Coal Spirals. Coal Preparation 14, 199–222.

Holland-Batt, A.B., 1995. The Dynamics of Sluice and Spiral Separations. Minerals Engineering 8 (1), 3–21.

Holland-Batt, A.B., 1998. Gravity Separation: A Revitalized Technology. Mining Engineering 50 (9), 43–48.

Holtham, P.N., 1990. Flow visualization of secondary currents on spiral separators. Minerals Engineering 5, 279–286.

Holtham, P.N., 1992a. Primary and secondary fluid velocities on spiral separators. Minerals Engineering 5, 79–91.

Holtham, P.N., 1992b. Particle transport in gravity concentrators and the bagnold effect. Minerals Engineering 5 (2), 205–221.

Kapur, P.C., Meloy, T.P., 1998. Spirals Observed. International Journal of Mineral Processing 53, 15–28.

Kapur, P.C., Meloy, T.P., 1999. Industrial modeling of spirals for optimal configuration and design: spiral geometry, fluid flow and forces on particles. Powder Technology 102, 244–252.

Krasnov, M., Kiselev, M., Makarenko, G., Shikin, E., 1990. Mathematical Analysis for Engineers. Mir Publishers, Moscow. (Chapter, 14–15).

Loveday, G.K., Cilliers, J.J., 1994. Fluid flow modelling on spiral concentrators. Minerals Engineering 7, 223–237.

MacNamara, L., Addison, F., Miles, N.J., Bethell, P., Davies, P., 1995. The Application of New Configurations of Coal Spirals, Proceedings, 12th International Coal Preparation Conference and Exhibit, Lexington, Kentucky, May 2–4, pp. 43–52.

MacNamara, L., Toney, T.A., Moorhead, R.G., Miles, N.J., Bethell, P., Everitt, B., 1996. On Site Testing of the Compound Spiral. Proceedings, 13th International Coal Preparation Conference and Exhibit, Lexington, Kentucky, April 30-May 2, pp. 110–121.

Mills, C., 1978. Process Design, Scale-Up and Plant Design for Gravity Concentration. Mineral Processing Plant Design. AIMME, New York, pp. 12–15.

Simons, D.B., Senturk, F., 1976. Sediment transport technology, Chap.7. Water Resources Publications, Littleton.

Sivamohan, S., Forssberg, E., 1985. Principles of spiral concentration, Int. J. Minerals Processing 15, 173–181.

Thompson, J.V., Welker, M., 1990. The Humphries Companies: Development and Application of Humphreys Spiral Concentrator. Skillings Mining Review, Feb. 24, pp. 4–15.

Von Seggern, D.H., 1990. CRC handbook of mathematical curves and surfaces. CRC Press, Boca Raton.

Walsh, D.E., Kelly, E.G., 1992. An Investigation of the Performance of a Spiral Using Radioactive Gold Tracers. Minerals and Metallurgical Processing 9 (3), 105–109.

Weldon, W.S., MacHunter, R.M.G., 1997. Recent Advances in Coal Spiral Development. SME Annual Meeting, Denver, Colorado, Preprint No. 97–82, Feb. 24–27.

Wills, B.A., 1992. Mineral Processing Technology, 5th edition. pp. 430–433.